

Strong Pauli paramagnetic effect in the upper critical field of $\text{KCa}_2\text{Fe}_4\text{As}_4\text{F}_2$

Teng Wang,^{1,2,3} Chi Zhang,^{1,2,4} Liangcai Xu,⁵ Jinhua Wang,⁵ Shan Jiang,⁵ Zengwei Zhu,⁵ Zhaosheng Wang,⁶ Jianan Chu,^{1,2,4} Jiaxin Feng,^{1,2,4} Lingling Wang,¹ Wei Li,⁷ Tao Hu,^{1,2} Xiaosong Liu,^{1,2,3} and Gang Mu^{1,2,*}

¹State Key Laboratory of Functional Materials for Informatics,
Shanghai Institute of Microsystem and Information Technology,
Chinese Academy of Sciences, Shanghai 200050, China

²CAS Center for Excellence in Superconducting Electronics(CENSE), Shanghai 200050, China

³School of Physical Science and Technology, ShanghaiTech University, Shanghai 201210, China

⁴University of Chinese Academy of Science, Beijing 100049, China

⁵Wuhan National High Magnetic Field Center and School of Physics,
Huazhong University of Science and Technology, Wuhan 430074, China

⁶Anhui Province Key Laboratory of Condensed Matter Physics at Extreme Conditions,
High Magnetic Field Laboratory of the Chinese Academy of Sciences, Hefei 230031, China

⁷Department of Physics and State Key Laboratory of Surface Physics, Fudan University, Shanghai 200433, China

Recently, 12442 system of Fe-based superconductors has attracted considerable attention owing to its unique double-FeAs-layer structure. A steep increase in the in-plane upper critical field with cooling has been observed near the superconducting transition temperature, T_c , in $\text{KCa}_2\text{Fe}_4\text{As}_4\text{F}_2$ single crystals. Herein, we report a high-field investigation on upper critical field of this material over a wide temperature range, and both out-of-plane ($H\parallel c$, H_{c2}^c) and in-plane ($H\parallel ab$, H_{c2}^{ab}) directions have been measured. A sublinear temperature-dependent behavior is observed for the out-of-plane H_{c2}^c , whereas strong convex curvature with cooling is observed for the in-plane H_{c2}^{ab} . Such behaviors could not be described by the conventional Werthamer–Helfand–Hohenberg (WHH) model. The data analysis based on the WHH model by considering the spin aspects reveals a large Maki parameter $\alpha = 9$, indicating that the in-plane upper critical field is affected by a very strong Pauli paramagnetic effect.

Keywords: 12442, upper critical field, Pauli paramagnetic effect

PACS numbers: 74.70.Xa, 72.20.Ht, 74.25.Op

1 Introduction

Unconventional superconductivity is closely related to the electronic and crystal structures of the materials¹. Adjustment of the crystal structure often leads to abundant physical manifestations^{2–5}. From this viewpoint, the 12442 system, which is the only system with two FeAs layers between neighboring insulating layers in Fe-based superconductors (FeSCs), has gained considerable attention in the field of superconducting (SC) materials^{6–15}. Depending on the detailed compositions, materials in this system are superconducting with $T_c = 28\text{--}37\text{ K}$ ^{6–10}. The recent advances in the field of high-quality single crystal growth have greatly promoted studies on the intrinsic physical properties of this system^{16–18}. For example, a large anisotropy of the upper critical field $\Gamma = H_{c2}^{ab}/H_{c2}^c$ and very steep increase of the in-plane H_{c2}^{ab} with cooling are observed in the temperature region near T_c in $\text{CsCa}_2\text{Fe}_4\text{As}_4\text{F}_2$ and $\text{KCa}_2\text{Fe}_4\text{As}_4\text{F}_2$ single crystals^{16,18}. These findings may be significant both for the fundamental physics and potential applications. Currently, however, the behavior at lower temperatures and higher magnetic fields is still unknown.

Generally, for type-II superconductors, the upper critical field can be affected by the interactions between the external magnetic field and orbital motion of the SC electrons, by the effect of the field on the electron spin magnetic moments (Pauli paramagnetic effect), and by the

spin-orbit scattering^{19–22}. In the case of FeSCs, the Pauli paramagnetic effect is significant, severely limiting the in-plane H_{c2}^{ab} when approaching zero temperature^{23–28}. Therefore, almost all the FeSCs exhibit isotropic characteristics in low temperature. Hence, the behavior of the upper critical field of 12442 system has gained great research interest. The pulsed magnetic field can provide a vital platform for studying this subject²⁹. In this study, we conducted an in-depth examination of the upper critical field of $\text{KCa}_2\text{Fe}_4\text{As}_4\text{F}_2$ single crystals using a pulsed magnetic field of up to 50 T. Strongly convex curvature with cooling was observed in the $H_{c2}^{ab} - T$ curve; this convexity interrupts the sharp upward trend of H_{c2} near T_c . The Werthamer–Helfand–Hohenberg model considering the spin aspects fitted the experimental data, and a significantly strong Pauli paramagnetic effect was revealed.

2 Materials and methods

The $\text{KCa}_2\text{Fe}_4\text{As}_4\text{F}_2$ single crystals were grown using the KAs self-flux method¹⁸. CaF_2 powder and home-made CaAs, KAs, and Fe_2As were mixed together in a stoichiometric ratio and placed in an alumina crucible; then, they were sealed in a stainless steel pipe³⁰. Fifteen times excess KAs was added as the flux. Moreover, appropriate amounts of CaAs and CaF_2 were added to suppress the formation of 122 phase KFe_2As_2 . The materials were heated at 980 °C for 20 h and cooled down to

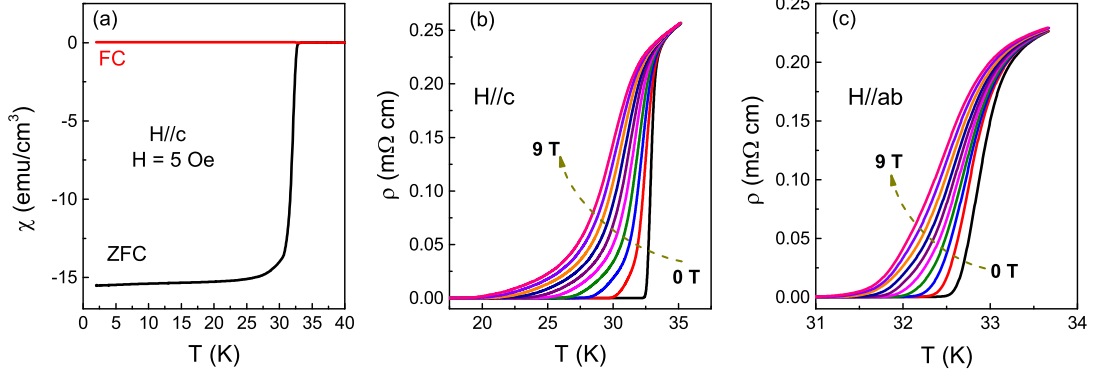


FIG. 1: (a) Magnetic susceptibility measured in zero-field-cooled (ZFC) and field-cooled (FC) modes. An external magnetic field of 5 Oe is applied along the c axis. (b)–(c) The temperature dependence of electronic resistivity under different magnetic fields up to 9 T with $H\parallel c$ and $H\parallel ab$, respectively. The interval for the field is 1 T/step.

900 °C at a rate of 1.6–4 °C/h, followed by rapid cooling to room temperature. The detailed characterizations of the samples has been reported in our previous work¹⁸.

Electronic resistivity was measured with a DC magnetic field of up to 9 T on a physical property measurement system (PPMS, Quantum Design). The experi-

ments were also conducted under the pulsed magnetic fields of up to 50 T. The magnetic fields were applied along the c -axis ($H\parallel c$) and ab -plane ($H\parallel ab$) of the crystals. Current was applied within the ab -plane and was perpendicular to the direction of the magnetic field. Magnetic susceptibility measurement was conducted using a magnetic property measurement system (MPMS, Quantum Design).

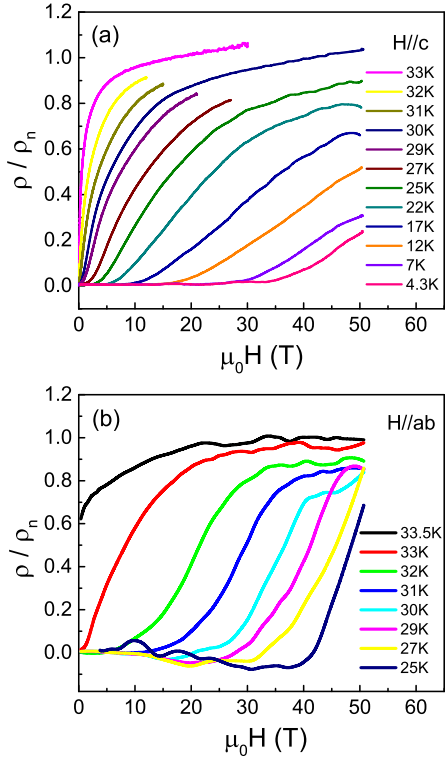


FIG. 2: Magnetic field dependence of resistivity at different temperatures for $\text{KCa}_2\text{Fe}_4\text{As}_4\text{F}_2$. The data are normalized to the value in the normal state ρ_n . The magnetic field is applied with two orientations (a) $H\parallel c$ and (b) $H\parallel ab$.

3 Results and discussion

In our previous work¹⁸, we reported that $\chi - T$ data measured with $H\parallel ab$ represents a superconducting volume fraction very close to 100%. Herein, we show the temperature dependence of magnetic susceptibility data $\chi - T$ with $H\parallel c$, see Fig. 1(a). The data reveals a very sharp SC transition at $T_c = 33.2$ K, indicating that our sample is of high quality and good homogeneity. The in-plane resistivity as a function of temperature was measured under different fields up to 9 T. In Figs. 1(b) and (c), we show the $\rho - T$ data with $H\parallel c$ and $H\parallel ab$, respectively. The SC transition displays a width of approximately 1 K under zero field, which is broadened by the external magnetic field. Such a broadening has been reported in 1111 system of FeSCs and cuprates, which is a consequence of the formation of a vortex-liquid state^{31–34}. Note that the scale of the x -coordinates for these two graphs are different, representing a clear anisotropy in the suppression of the SC transition by the magnetic field. Because of the limitation of the magnetic field, we only obtained information in a very narrow temperature region near T_c . Hence, we conducted transport measurements under the pulsed magnetic fields of up to 50 T.

Normalized resistivity as a function of pulsed magnetic field is shown in Figs. 2(a) and (b). With the decrease of temperature, the SC state can survive under a higher

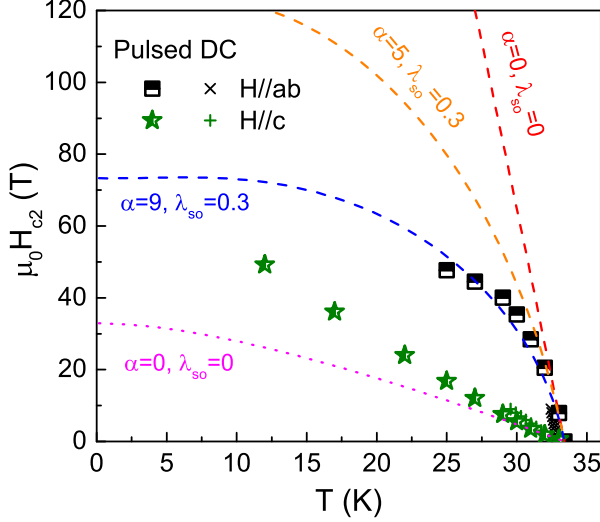


FIG. 3: Upper critical field $\mu_0 H_{c2}(T)$ versus temperature for $\text{KCa}_2\text{Fe}_4\text{As}_4\text{F}_2$ single crystals. Half-filled symbols and crosses represent the data obtained in the pulsed field and low magnetic field, respectively. The dashed and dotted lines are the WHH fits for the experimental data with $H\parallel ab$ and $H\parallel c$, respectively.

field. In the case of $H\parallel c$ (see Fig. 2(a)), the SC transition becomes broadening in the low temperature region, indicating a wide area of the vortex-liquid state. This is consistent with the observations shown in Fig. 1(b). As shown in Fig. 2(b), such a broadening behavior is not observed in the case of $H\parallel ab$. This difference in behavior is a consequence of the different types of vortices in the different field orientations in a quasi-two-dimensional layered material³⁵. It is believed that the presence of SC fluctuation near the onset of the SC transition and vortex-liquid state near zero-resistivity will affect the determination of upper critical field^{27,28}. Hence, the criteria $50\%\rho_n$ was adopted herein. The normal state resistivity ρ_n was determined from the $\rho-T$ curve under zero field.

The upper critical fields for the two orientations, H_{c2}^{ab} and H_{c2}^c , as a function of temperature are shown in Fig. 3. The data from the pulsed field and DC field experiments are roughly consistent. We first checked the behavior of in-plane $H_{c2}^{ab}(T)$. Adjacent to the SC transition T_c , $H_{c2}^{ab}(T)$ shows a steep increase with cooling leading to a slope $H' = -d\mu_0 H_{c2}^{ab}/dT|_{T_c} = 19.4$ T/K. This value is smaller than that obtained using the criteria $90\%\rho_n$ ¹⁸ because of the broadening effect induced by the magnetic field. As the temperature decreases further, this steep tendency is interrupted severely, and the $H_{c2}^{ab}-T$ curve reveals strongly convex curvature in the temperature region 25–30 K. On the contrary, the out-of-plane $H_{c2}^c(T)$ shows a linear temperature-dependent behavior in fields exceeding 8 T. Below 8 T, the H_{c2}^c-T curve displays a tail-like feature with a low slope. Similar features are also observed in other systems of FeSCs^{27,28,36}.

To comprehensively evaluate the effects of the orbital pair-breaking effect, spin-paramagnetic pair-breaking effect, and spin-orbit interaction on the upper critical field, we checked our data based on the WHH theory²². In the dirty limit, according to the WHH theory, the upper critical field can be obtained from the function²²

$$\ln \frac{1}{t} = \sum_{\nu=-\infty}^{\infty} \left\{ \frac{1}{|2\nu+1|} - [|2\nu+1| + \frac{\bar{h}}{t} + \frac{(\alpha\bar{h}/t)^2}{|2\nu+1| + (\bar{h} + \lambda_{so})/t}]^{-1} \right\}, \quad (1)$$

where $t = T/T_c$, $\bar{h} = 4H_{c2}/(\pi^2 H' T_c)$, and α and λ_{so} are parameters reflecting the strength of the spin paramagnetic effect and spin-orbit interaction, respectively. The parameter α was proposed by Maki, known as Maki parameter¹⁹. For the orientation of $H\parallel ab$, the conventional scenario without spin-paramagnetic effect and spin-orbit interaction ($\alpha = 0$, $\lambda_{so} = 0$) could not describe the experimental data (see the red dashed line in Fig. 3); the conventional scenario gives an estimation exceeding thrice the experimental value at 25 K. By adjusting the values of α and λ_{so} , the data can be roughly represented by the theoretical model with the parameters $\alpha = 9$ and $\lambda_{so} = 0.3$, as shown by blue dashed line in Fig. 3. Note that the value of α obtained herein is very large, and the previous maximum value of $\alpha = 6.5$ is found in the 1111 system²⁸. This indicates a very strong spin-paramagnetic effect in the present system. Meanwhile, the spin-orbit interaction with a strength $\lambda_{so} = 0.3$ is essential to describe the experimental data. To give a vivid impression for the necessity of such a large α , we also show the theoretical curve with $\alpha = 5$ and $\lambda_{so} = 0.3$, as shown by yellow dashed line in Fig. 3, which fails to reflect the strongly convex curvature at approximately 25 K.

In the case of out-of-plane case ($H\parallel c$), as shown by pink dotted line in Fig. 3, the conventional WHH model again fails to describe the experimental data. Moreover, the theoretical curve is below the experimental data. This means that the introduction of α and λ_{so} can not improve the situation because typically the spin-paramagnetic effect further suppresses the value of the upper critical field²². We note that this sublinear feature of the $H_{c2}^c - T$ is common in the family of FeSCs and is widely believed to be a consequence of the multiband effect^{27,28}. The feature of multiband effect is more pronounced for the orientation with $H\parallel c$ than that with $H\parallel ab$. The ratio $\eta = D_h/D_e$, where D_h and D_e are the diffusivities of the hole and electronic bands respectively, is the key factor controlling the $H_{c2} - T$ behavior of the multiband superconductors in the dirty limit^{37–39}. Typically, the in-plane value D_h^{ab} is much smaller than D_e^{ab} because of the large effective mass of the hole-type carriers. When the field is applied along the c axis, only the in-plane diffusivity is involved. Hence, we obtain a quite small value of η , leading to the pronounced feature of the multiband effect. For $H\parallel ab$, on the contrary, the out-of-plane values of D_h^c and D_e^c should be considered when

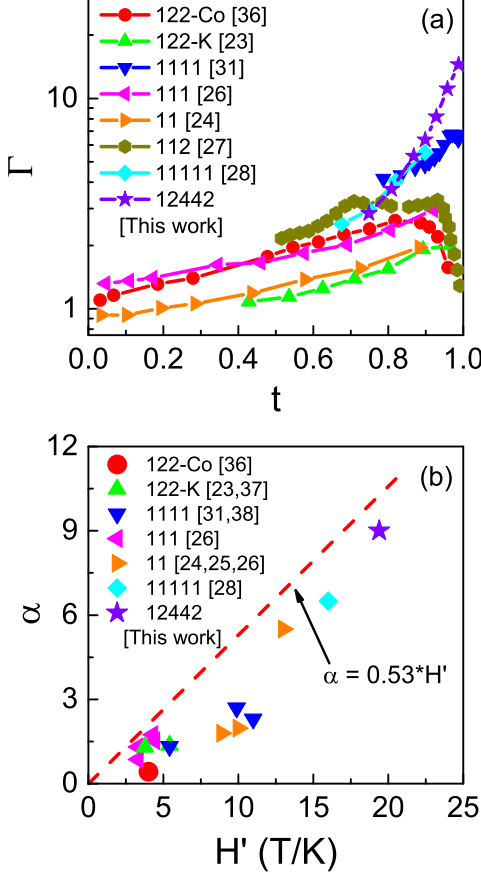


FIG. 4: (a) Anisotropic parameter $\Gamma = H_{c2}^{ab}/H_{c2}^c$ as a function of the reduced temperature $t = T/T_c$. (b) The spin Maki parameter α as a function of the slope $H' = -d\mu_0 H_{c2}^{ab}/dT|_{T_c}$. Red dashed line denotes the Maki relation in the weak-coupling limit. The references for the data are denoted in the figure.

calculating η , and hence, η is enhanced. This may explain the observed indistinctive multiband feature in the case of $H \parallel ab$. Such a tendency was noticed and discussed by Hunte et al. when studying the $\text{LaFeAsO}_{0.89}\text{F}_{0.11}$ system³⁹.

Finally, we performed a quantitative comparison of the studied system with other systems of FeSCs^{23–28,32,40–42}. In Fig. 4(a), the anisotropic parameter Γ is plotted as a function of the reduced temperature $t = T/T_c$ for different FeSCs including 122, 1111, 111, 11, 112, 11111, and the present 12442 system. It is interesting that all the curves share a common tendency toward $\Gamma \simeq 1$ as the temperature approaches 0 K. The present $\text{KCa}_2\text{Fe}_4\text{As}_4\text{F}_2$ system also follows this general trend. The difference in the case of 12442 material is that it has a larger value of Γ near T_c ($t = 1$), which reveals a steeper decrease with cooling. Next, we checked the Maki parameter α .

According to the Maki formula¹⁹, α can be expressed as

$$\alpha = \frac{\sqrt{2}H_{c2}^{Orb}(0)}{H_P(0)}, \quad (2)$$

where $H_{c2}^{Orb}(0) = 0.693 \times H' \times T_c$ is the upper critical field in the absence of the spin term, and $H_P(0)$ is the Pauli limited field. In the weakly coupled BCS scenario, we have $H_P^{BCS}(0) = 1.84 \times T_c$. Therefore, a very simple relation $\alpha = 0.53H'$ can be obtained if H' is expressed in units of T/K. This relation, which is represented by the red dashed line in Fig. 4(b), reveals the close relation between α and slope of H_{c2} vs T at T_c . The experimental data roughly follows the tendency of the Maki formula. The departure of the data from the red dashed line is a consequence of the enhancement of $H_P(0)$ over $H_P^{BCS}(0)$ due to the strong coupling effect. The present 12442 system also exhibits this tendency to a greater extent than that in the other FeSC systems.

The value of α can be determined using the physical quantities in the normal state²²:

$$\alpha \propto \gamma_n \rho_n, \quad (3)$$

where γ_n and ρ_n are the normal state electronic specific heat (SH) coefficient and normal state dc resistivity, respectively. This may provide clues for exploring the origin of the large α in $\text{KCa}_2\text{Fe}_4\text{As}_4\text{F}_2$. The SH measurements revealed a rather high SH jump $\Delta C/T|_{T_c} = 32.5 - 37.5$ mJ/mol-Fe K² in $\text{KCa}_2\text{Fe}_4\text{As}_4\text{F}_2$ ^{6,43}; this value is the second-largest after the value for the K-doped 122 system $\text{Ba}_{0.6}\text{K}_{0.4}\text{Fe}_2\text{As}_2$ (~ 49 mJ/mol-Fe K²)⁴⁴ in the family of FeSCs. This suggests a large magnitude of γ_n in $\text{KCa}_2\text{Fe}_4\text{As}_4\text{F}_2$, assuming a proportional relationship between γ_n and $\Delta C/T|_{T_c}$. From the viewpoint of the normal state dc resistivity, ρ_n of $\text{KCa}_2\text{Fe}_4\text{As}_4\text{F}_2$ is thrice (5 times) that of $\text{Ba}_{0.6}\text{K}_{0.4}\text{Fe}_2\text{As}_2$ at 300 K (40K)^{18,44}. In other FeSCs systems, e.g., the 1111 system, the value of ρ_n is large, whereas γ_n is small^{45,46}. Considering the above two factors synthetically and comprehensively, we find that the large value of α in $\text{KCa}_2\text{Fe}_4\text{As}_4\text{F}_2$ can be attributed qualitatively to the fact that both γ_n and ρ_n are relatively larger.

4 Conclusions

In summary, the high magnetic field dependence of the resistivity for the $\text{KCa}_2\text{Fe}_4\text{As}_4\text{F}_2$ single crystals was measured. The extremely steep increase of in-plane H_{c2}^{ab} with cooling near T_c changes to a bending behavior, resulting in a rapid decrease in the anisotropy Γ with cooling. The evolution feature of the $H_{c2}^{ab} - T$ curve can only be described by the WHH model with a large Maki parameter $\alpha = 9$, indicating a strong Pauli paramagnetic effect in the present system. The relatively large γ_n and ρ_n may explain the observed large value of α .

This work is supported by the Youth Innovation Promotion Association of the Chinese Academy of Sciences

(No. 2015187), the National Natural Science Foundation of China (Nos. 11204338, 11704385 and 11874359), and the "Strategic Priority Research Program (B)" of the

Chinese Academy of Sciences (No. XDB04040300). We thank Dr. X. Z. Xing for the help when handling the WHH model.

-
- * mugang@mail.sim.ac.cn
- ¹ H. C. Xu, X. H. Niu, Z. R. Ye, and D. L. Feng, *Acta Phys. Sin.* **67**, 207405 (2018).
 - ² Y. Kamihara, T. Watanabe, M. Hirano, and H. Hosono, *J. Am. Chem. Soc.* **130**, 3296 (2008).
 - ³ X. Zhu, F. Han, G. Mu, P. Cheng, B. Shen, B. Zeng, and H.-H. Wen, *Phys. Rev. B* **79**, 220512(R) (2009).
 - ⁴ F.-C. Hsu, J.-Y. Luo, K.-W. Yeh, T.-K. Chen, T.-W. Huang, P. M. Wu, Y.-C. Lee, Y.-L. Huang, Y.-Y. Chu, D.-C. Yan, et al., *Natl. Acad. Sci.* **105**, 14262 (2008).
 - ⁵ M. Rotter, M. Tegel, and D. Johrendt, *Phys. Rev. Lett.* **101**, 107006 (2008).
 - ⁶ Z.-C. Wang, C.-Y. He, S.-Q. Wu, Z.-T. Tang, Y. Liu, A. Ablimit, C.-M. Feng, and G.-H. Cao, *J. Am. Chem. Soc.* **138**, 7856 (2016).
 - ⁷ Z. Wang, C. He, Z. Tang, S. Wu, and G. Cao, *Sci. China Mater.* **60**, 83 (2017).
 - ⁸ Z.-C. Wang, C.-Y. He, S.-Q. Wu, Z.-T. Tang, Y. Liu, A. Ablimit, Q. Tao, C.-M. Feng, Z.-A. Xu, and G.-H. Cao, *J. Phys.: Condens. Matt.* **29**, 11LT01 (2017).
 - ⁹ Z.-C. Wang, C.-Y. He, S.-Q. Wu, Z.-T. Tang, Y. Liu, and G.-H. Cao, *Chem. Mater.* **29**, 1805 (2017).
 - ¹⁰ S.-Q. Wu, Z.-C. Wang, C.-Y. He, Z.-T. Tang, Y. Liu, and G.-H. Cao, *Phys. Rev. Materials* **1**, 044804 (2017).
 - ¹¹ G. Wang, Z. Wang, and X. Shi, *Europhys. Lett.* **116**, 37003 (2016).
 - ¹² J. Ishida, S. Iimura, and H. Hosono, *Phys. Rev. B* **96**, 174522 (2017).
 - ¹³ F. K. K. Kirschner, D. T. Adroja, Z.-C. Wang, F. Lang, M. Smidman, P. J. Baker, G.-H. Cao, and S. J. Blundell, *Phys. Rev. B* **97**, 060506(R) (2018).
 - ¹⁴ D. T. Adroja, F. K. K. Kirschner, F. Lang, M. Smidman, A. D. Hillier, Z.-C. Wang, G.-H. Cao, G. B. G. Stenning, and S. J. Blundell, *J. Phys. Soc. Jpn.* **87**, 124705 (2018).
 - ¹⁵ B. Wang, Z.-C. Wang, K. Ishigaki, K. Matsubayashi, T. Eto, J. Sun, J.-G. Cheng, G.-H. Cao, and Y. Uwatoko, *Phys. Rev. B* **99**, 014501 (2019).
 - ¹⁶ Z. C. Wang, Y. Liu, S. Q. Wu, Y. T. Shao, Z. Ren, and G. H. Cao, *Phys. Rev. B* **99**, 144501 (2019).
 - ¹⁷ Y. Y. Huang, Z. C. Wang, Y. J. Yu, J. M. Ni, Q. Li, E. J. Cheng, G. H. Cao, and S. Y. Li, *Phys. Rev. B* **99**, 020502(R) (2019).
 - ¹⁸ T. Wang, J. Chu, H. Jin, J. Feng, L. Wang, Y. Song, C. Zhang, X. Xu, W. Li, Z. Li, et al., *J. Phys. Chem. C* **123**, 13925 (2019).
 - ¹⁹ K. Maki, *Physics Physique Fizika* **1**, 127 (1964).
 - ²⁰ K. Maki, *Phys. Rev.* **148**, 362 (1966).
 - ²¹ E. Helfand and N. R. Werthamer, *Phys. Rev.* **147**, 288 (1966).
 - ²² N. R. Werthamer, E. Helfand, and P. C. Hohenberg, *Phys. Rev.* **147**, 295 (1966).
 - ²³ H. Q. Yuan, J. Singleton, F. F. Balakirev, S. A. Baily, G. F. Chen, J. L. Luo, and N. L. Wang, *Nature* **457**, 565 (2009).
 - ²⁴ M. Fang, J. Yang, F. F. Balakirev, Y. Kohama, J. Singleton, B. Qian, Z. Q. Mao, H. Wang, and H. Q. Yuan, *Phys. Rev. B* **81**, 020509 (2010).
 - ²⁵ S. Khim, J. W. Kim, E. S. Choi, Y. Bang, M. Nohara, H. Takagi, and K. H. Kim, *Phys. Rev. B* **81**, 184511 (2010).
 - ²⁶ S. Khim, B. Lee, J. W. Kim, E. S. Choi, G. R. Stewart, and K. H. Kim, *Phys. Rev. B* **84**, 104502 (2011).
 - ²⁷ X. Z. Xing, W. Zhou, J. H. Wang, Z. W. Zhu, Y. F. Zhang, N. Zhou, B. Qian, X. F. Xu, and Z. X. Shi, *Sci. Rep.* **7**, 45943 (2017).
 - ²⁸ Z. Wang, J. Yuan, J. Wosnitza, H. Zhou, Y. Huang, K. Jin, F. Zhou, X. Dong, and Z. Zhao, *J. Phys.: Condens. Matt.* **29**, 025701 (2017).
 - ²⁹ Y. Ma, G. Mu, T. Hu, Z. Zhu, Z. Li, W. Li, Q. Ji, X. Zhang, L. Wang, and X. Xie, *Sci. China Phys. Mech.* **61**, 127408 (2018).
 - ³⁰ K. Kihou, T. Saito, S. Ishida, M. Nakajima, Y. Tomioka, H. Fukazawa, Y. Kohori, T. Ito, S.-i. Uchida, A. Iyo, et al., *J. Phys. Soc. Jpn.* **79**, 124713 (2010).
 - ³¹ J. Jaroszynski, F. Hunte, L. Balicas, Y.-j. Jo, I. Raičević, A. Gurevich, D. C. Larbalestier, F. F. Balakirev, L. Fang, P. Cheng, et al., *Phys. Rev. B* **78**, 174523 (2008).
 - ³² H.-S. Lee, M. Bartkowiak, J.-H. Park, J.-Y. Lee, J.-Y. Kim, N.-H. Sung, B. K. Cho, C.-U. Jung, J. S. Kim, and H.-J. Lee, *Phys. Rev. B* **80**, 144512 (2009).
 - ³³ W. K. Kwok, S. Fleshler, U. Welp, V. M. Vinokur, J. Downey, G. W. Crabtree, and M. M. Miller, *Phys. Rev. Lett.* **69**, 3370 (1992).
 - ³⁴ H. Safar, P. L. Gammel, D. A. Huse, D. J. Bishop, J. P. Rice, and D. M. Ginsberg, *Phys. Rev. Lett.* **69**, 824 (1992).
 - ³⁵ G. Blatter, M. V. Feigel'man, V. B. Geshkenbein, A. I. Larkin, and V. M. Vinokur, *Rev. Mod. Phys.* **66**, 1125 (1994).
 - ³⁶ A. Pisoni, S. Katrych, P. Szirmai, B. Náfrádi, R. Gaál, J. Karpinski, and L. Forró, *J. Phys.: Condens. Matt.* **28**, 115701 (2016).
 - ³⁷ A. Gurevich, *Phys. Rev. B* **67**, 184515 (2003).
 - ³⁸ A. Gurevich, *Physica C: Superconductivity* **456**, 160 (2007).
 - ³⁹ F. Hunte, J. Jaroszynski, A. Gurevich, D. C. Larbalestier, R. Jin, A. S. Sefat, M. A. McGuire, B. C. Sales, D. K. Christen, and D. Mandrus, *Nature* **453**, 903 (2008).
 - ⁴⁰ M. Kano, Y. Kohama, D. Graf, F. Balakirev, A. S. Sefat, M. A. McGuire, B. C. Sales, D. Mandrus, and S. W. Tozer, *J. Phys. Soc. Jpn.* **78**, 084719 (2009).
 - ⁴¹ T. Terashima, M. Kimata, H. Satsukawa, A. Harada, K. Hazama, S. Uji, H. Harima, G.-F. Chen, J.-L. Luo, and N.-L. Wang, *J. Phys. Soc. Jpn.* **78**, 063702 (2009).
 - ⁴² G. Fuchs, S.-L. Drechsler, N. Kozlova, G. Behr, A. Köhler, J. Werner, K. Nenkov, R. Klingeler, J. Hamann-Borrero, C. Hess, et al., *Phys. Rev. Lett.* **101**, 237003 (2008).
 - ⁴³ T. Wang, J. N. Chu, J. X. Feng, L. L. Wang, X. G. Xu, W. Li, H. H. Wen, X. S. Liu, and G. Mu, *arXiv:1903.09447* (2019).
 - ⁴⁴ G. Mu, H. Luo, Z. Wang, L. Shan, C. Ren, and H.-H. Wen, *Phys. Rev. B* **79**, 174501 (2009).
 - ⁴⁵ Y. H. Ma, K. K. Hu, Q. C. Ji, B. Gao, H. Zhang, G. Mu, F. Q. Huang, and X. M. Xie, *J. Cryst. Growth* **451**, 161 (2016).

- ⁴⁶ J. N. Chu, T. Wang, Y. H. Ma, J. X. Feng, L. L. Wang, X. G. Xu, W. Li, G. Mu, and X. M. Xie, J. Phys.: Condens. Matter **31**, 455602 (2019).